Effects of Chemical Reactions in the Hypersonic Reacting Flow around Blunt Bodies

ZHAO Faming, WANG Jiangfeng, FAN Xiaofeng, YANG Tianpeng*

College of Aerospace Engineering, Nanjing University of Aeronautics and Astronautics, Nanjing 210016, P. R. China

(Received 9 May 2017; revised 5 September 2017; accepted 15 September 2017)

Abstract: The effects of chemical reactions in the hypersonic reacting flow are investigated using an integrated algorithm considering simultaneously two different reaction mechanisms, i.e., including the high temperature air non-equilibrium chemical reactions and the H_2-air combustion reactions. The program is validated by the air non-equilibrium flow at Mach number of 25.9 with the RAM C-II configuration and the shock-induced combustion flow at Mach number of 4.512 6 around a sphere, respectively. Furthermore, the mixed reacting flow with the Mach number of 10.0 with an opposing jet of hydrogen is numerically analyzed. The results show that the program is reliable, and the effects of chemical reactions engender in the decrease of peak temperature along characteristic lines, as well as on the surface. The production of water is augmented in the region with high ratio of oxygen to hydrogen and weakened in the area with low ratio of oxygen to hydrogen by the air chemical non-equilibrium effects.

Key words: hypersonic; air chemical non-equilibrium; combustion; effects of chemical reaction

CLC number: V211.3 **Document code**: A **Article ID**: 1005-1120(2019)01-0071-09

0 Introduction

The high-temperature air surrounding the hypersonic vehicles undergoes chemical non-equilibrium processes, such as the dissociation, vibrational excitation and ionization during the reentering period[1-4]. The effects of air chemical non-equilibrium have to be considered in the numerical prediction and engineering estimation[5-6]. Advances in the numerical simulation of air non-equilibrium flow have been obtained and hence greatly enhanced the analysis of difference and influence derived from various chemical reaction models and temperature models[7-9]. Meanwhile, the hypersonic cruise vehicles are equipped with the propulsion system and reaction control system of rocket or scramjet engine in general. Therefore, the effects of combustion of the hydrogen or hydrocarbon fuel[10] should be considered, too. Commercial software, such as FLUENT, and self-developed program, such as UNCOMB[11], can be used to compute the combustion flow.

Nevertheless, the numerical investigations of the air non-equilibrium flow and combustion flow are conducted independently at present. The interaction effects of the air chemical non-equilibrium and combustion are unpredictable. For example, changing of the concentrations of oxygen and oxygen atoms near the inlet of the air-breathing vehicles because of the air chemical reactions affect the combustion reactions inside the combustion chamber. Thus, it is necessary to consider simultaneously the effects of the air chemical non-equilibrium and combustion of the advanced hypersonic vehicles, such as X-43, X-51, HTV-2, and some other air-breathing missiles[12-13].

In this paper, a program for computing the hypersonic reacting flow is developed, considering simultaneously the air chemical reactions and combustion reactions . As no experimental or computational

*Corresponding author, E-mail: wangjf@nuaa.edu.cn.

How to cite this article: ZHAO Faming, WANG Jiangfeng, FAN Xiaofeng, et al. Effects of Chemical Reactions in the Hypersonic Reacting Flow around Blunt Bodies[J]. Transactions of Nanjing University of Aeronautics and Astronautics, 2019, 36(1):71-79.

http://dx.doi.org/10.16356/j.1005-1120.2019.01.006

data can be found about the mixed reacting flow, the hypersonic air non-equilibrium flow around the RAM-C II configuration and the supersonic shock-induced combustion flow around a sphere are conducted respectively for the validation of the numerical algorithm. Furthermore, the hypersonic reacting flow with an opposing jet of hydrogen around a sphere is performed to study the interaction effects of air chemical non-equilibrium and combustion.

1 Computational Method

1.1 Governing equations

The axisymmetric multi-species Navier-Stokes (N-S) equations in conservation form can be expressed in the Cartesian coordinates as[14]

$$\frac{\partial \boldsymbol{U}}{\partial t}+\frac{\partial \boldsymbol{E}}{\partial x}+\frac{\partial \boldsymbol{F}}{\partial y}+\boldsymbol{H}=\frac{\partial \boldsymbol{E}_v}{\partial x}+\frac{\partial \boldsymbol{F}_v}{\partial y}+\boldsymbol{H}_v+\boldsymbol{\omega} \tag{1}$$

$$\boldsymbol{U}=\begin{bmatrix}\rho_1\\ \vdots\\ \rho_{ns}\\ \rho u\\ \rho v\\ e_t\end{bmatrix},\ \boldsymbol{E}=\begin{bmatrix}\rho_1 u\\ \vdots\\ \rho_{ns}u\\ \rho u^2+p\\ \rho uv\\ (e_t+p)u\end{bmatrix},\ \boldsymbol{F}=\begin{bmatrix}\rho_1 v\\ \vdots\\ \rho_{ns}v\\ \rho uv\\ \rho v^2+p\\ (e_t+p)v\end{bmatrix} \tag{2}$$

$$\boldsymbol{\omega}=\begin{bmatrix}\dot{\omega}_1\\ \vdots\\ \dot{\omega}_{ns}\\ 0\\ 0\\ 0\end{bmatrix},\ \boldsymbol{E}_v=\begin{bmatrix}\rho_1 D_1\dfrac{\partial c_1}{\partial x}\\ \vdots\\ \rho_{ns}D_{ns}\dfrac{\partial c_{ns}}{\partial x}\\ \tau_{xx}\\ \tau_{xy}\\ u\tau_{xx}+v\tau_{xy}+\lambda\dfrac{\partial T}{\partial x}\end{bmatrix}$$

$$\boldsymbol{F}_v=\begin{bmatrix}\rho_1 D_1\dfrac{\partial c_1}{\partial y}\\ \vdots\\ \rho_{ns}D_{ns}\dfrac{\partial c_{ns}}{\partial y}\\ \tau_{yx}\\ \tau_{yy}\\ u\tau_{yx}+v\tau_{yy}+\lambda\dfrac{\partial T}{\partial y}\end{bmatrix} \tag{3}$$

$$\boldsymbol{H}=\frac{1}{y}\begin{bmatrix}\rho_1 v\\ \vdots\\ \rho_{ns}v\\ \rho uv\\ \rho v^2\\ (e_t+p)v\end{bmatrix},\boldsymbol{H}_v=\frac{1}{y}\begin{bmatrix}\rho_1 D_1\dfrac{\partial c_1}{\partial y}\\ \vdots\\ \rho_{ns}D_{ns}\dfrac{\partial c_{ns}}{\partial y}\\ \tau_{yx}\\ \tau_{yy}-\tau_{\theta\theta}\\ u\tau_{yx}+v\tau_{yy}+\lambda\dfrac{\partial T}{\partial y}\end{bmatrix} \tag{4}$$

$$\tau_{xx}=\frac{2}{3}\mu\left(2\frac{\partial u}{\partial x}-\frac{\partial v}{\partial y}-\frac{u}{y}\right) \tag{5}$$

$$\tau_{yy}=\frac{2}{3}\mu\left(2\frac{\partial v}{\partial y}-\frac{\partial u}{\partial x}-\frac{v}{y}\right) \tag{6}$$

$$\tau_{xy}=\mu\left(\frac{\partial u}{\partial y}+\frac{\partial v}{\partial x}\right) \tag{7}$$

$$\tau_{yy}-\tau_{\theta\theta}=2\mu\left(\frac{\partial v}{\partial y}-\frac{v}{y}\right) \tag{8}$$

where $\rho, p, T, e_t, \mu, \lambda$ are the density, pressure, temperature, total energy per unit volume, viscosity, and thermal conductivity of the gas mixture, respectively; ρ_i, c_i, D_i are the density, mass concentration, and coefficients of mass diffusion of species, resperctively. The pressure of the gas mixture is obtained from the Dalton law[15] and the total energy per unit volume can be expressed as

$$p=\sum_{i=1}^{ns}\rho_i\frac{R_u}{M_i}T \tag{9}$$

$$e_t=\sum_{i=1}^{ns}\rho_i h_i+\frac{1}{2}\rho(u^2+v^2)-p \tag{10}$$

where M_i, h_i are the molecular weight and static enthalpy of species; and R_u the universal gas constant.

An integrated algorithm for computing the mixed reacting flow with air chemical reactions and H_2-air combustion reactions is developed, using the finite volume method based on the hybrid grid techniques. The central scheme with artificial dissipation is used for calculating the inviscid flux and the multistage Runge-Kutta scheme is employed for temporal discretisation. The turbulence model adopted here is the Spalart-Allmaras one-equation model. The program is compiled and verified on a 128-CPUs Linux system employing the memory-distributed parallel computing techniques.

1.2 Chemical kinetic model

For NR possible chemical reactions with NS species, the chemical reactions in a general form are[7]

$$\sum_{i=1}^{NJ}\alpha_{i,r}X_i \underset{k_{b,r}}{\overset{k_{f,r}}{\rightleftarrows}} \sum_{i=1}^{NJ}\beta_{i,r}X_i \tag{11}$$

where $r=1,2,\cdots,NR$ and NJ is equal to the sum of the reacting species (NS) plus the number of catalytic bodies; $\alpha_{i,r},\beta_{i,r}$ are the stoichiometric coefficients of the species on the rth reaction. X_i is the concentration of the chemical species and catalytic bodies in moles per unit volume, and $k_{f,r},k_{b,r}$ are the rates of forward and backward reactions, respectively. The net mass production per unit volume is

$$\dot{\omega}_i = M_i\sum_{r=1}^{NR}(\beta_{i,r}-\alpha_{i,r})\left(k_{f,r}\prod_{j=1}^{NJ}(\gamma_j\rho)^{\alpha_{j,r}} - k_{b,r}\prod_{j=1}^{NJ}(\gamma_j\rho)^{\beta_{j,r}}\right) \tag{12}$$

where γ_s is the mole mass ratio.

2 Results and Discussion

2.1 Hypersonic air non-equilibrium flow

The RAM C-II configuration illustrated in Ref. [16] is used in this case, with a 129×110 structured grid shown in Fig.1. The flight altitude is 71 km and the free stream is composed by the species of N_2 and O_2; the associated conditions are given in Table 1. The temperature of the wall is maintained at 1 500 K which is assumed to be non-catalytic. The chemical reaction model adopted is the 7-species (O_2, N_2, O, N, NO, NO^+, e^-) model with seven reaction equations proposed by Gupta[7], and the corresponding reaction coefficients are given in Ref.[2].

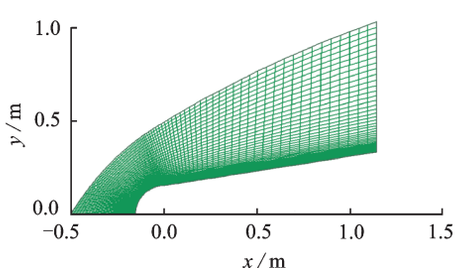

Fig.1 Computational grid

Table 1 Free stream conditions

Ma_∞	p_∞/Pa	T_∞/K	C_{N_2}	C_{O_2}
25.9	4.9	219.58	0.791 2	0.208 8

Fig.2 shows the comparison of the peak electron number density as a function of the normalized axial length (x/r). A value of $x/r=0$ represents the nose stagnation point. The experimental data shows that the electron number density is highest at the nose and falls off rapidly around the shoulder of the body, and the computational approximation follows this trend, but the fixed-wall temperature used in the calculation may be too high that would produce much more number of electrons near the wall. Fig. 3 shows the comparison of the normalized surface pressure distributions (p/p_∞) as a function of the normalized distance from the nose (D/r). The surface pressure distributions of the test match well with the Candler's work[1].

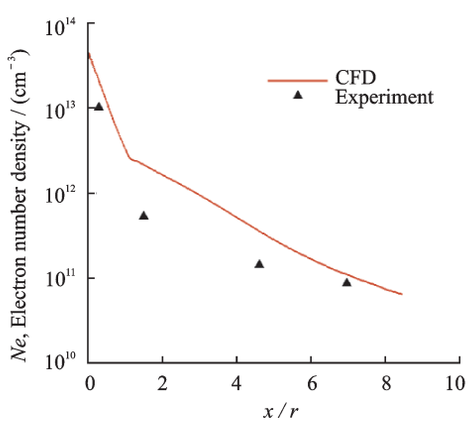

Fig.2 Comparison of peak electron number density

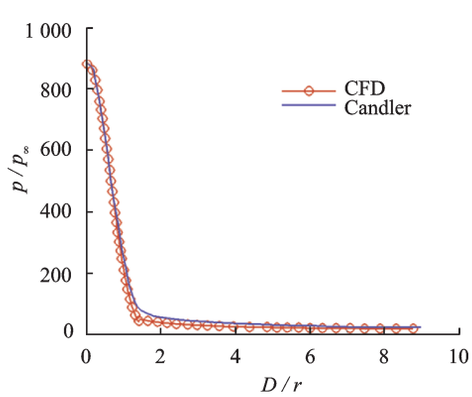

Fig.3 Comparison of surface pressure distributions

2.2 Shock-induced combustion flow

The radius of the sphere is 7.5 mm, and a

101×301 structured grid is generated for computation (Fig. 4). The free stream is composed by the species of H_2, O_2, and N_2, with the mole ratio $n(H_2):n(O_2):n(N_2)=2:1:3.76$; the associated conditions are given in Table 2. The wall is assumed to be adiabatic and non-catalytic. The chemical reaction model adopted is the 7-species (H_2, O_2, H_2O, O, H, OH, N_2) model with seven reaction equations by Shang[17], and the corresponding reaction coefficients are given in Ref. [17].

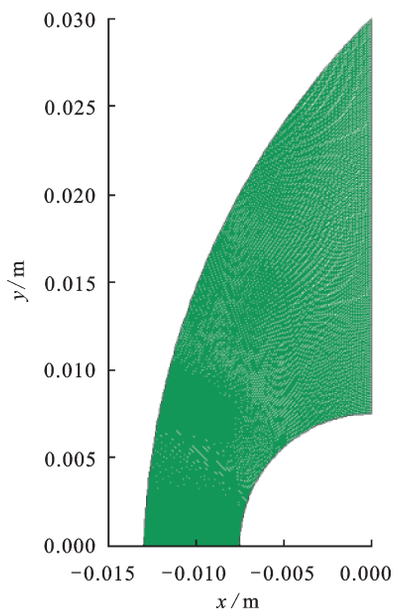

Fig.4 Computational grid

Table 2 Free stream conditions

Ma_∞	p_∞/Pa	T_∞/K
4.512 6	42 662	250

The comparison of the temperature distributions obtained from the test is presented in Fig. 5, where the uncoupled shock-deflagration phenomenon can be observed. The temperature after the shock wave is not high enough for the ignition of H_2, thus the combustion occurs after a period of induction. The shock wave and the deflagration wave are separated by the induced region clearly. The position of the shock wave matches well with the experimental results[18], and the position of the deflagration wave agrees well with that in Ref. [19].

Fig.6(a) shows the comparison of the pressure and temperature distributions along the stagnation

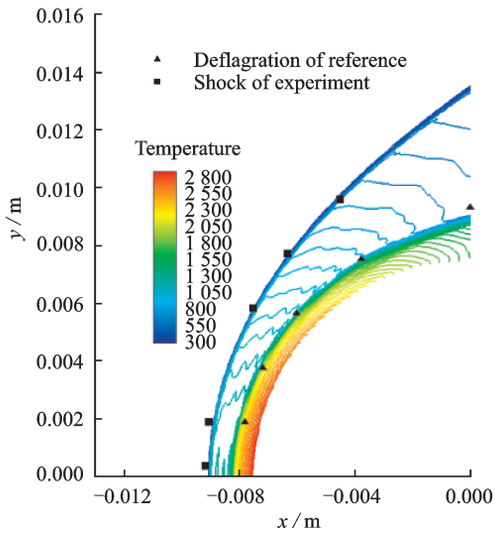

Fig.5 Comparison of temperature distributions

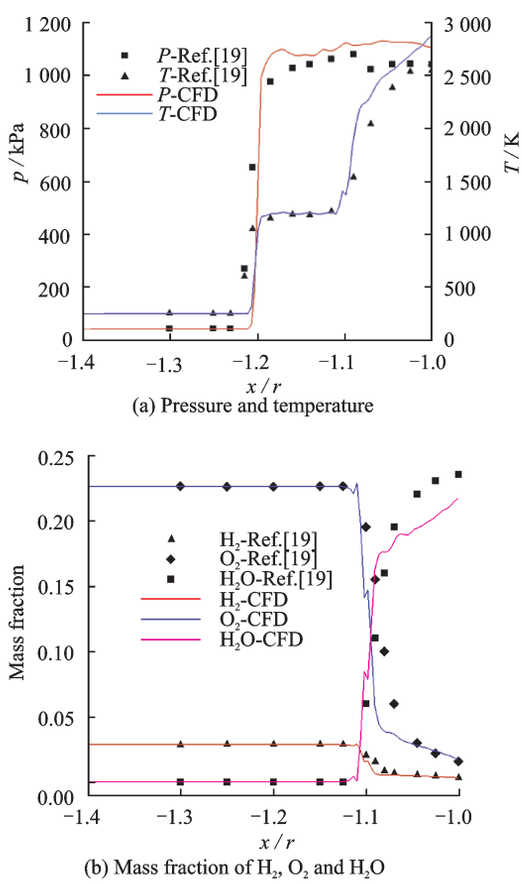

Fig.6 Comparison of parameter distributions along the stagnation line

line as a function of the normalized axial length x/r. A value of $x/r=-1$ represents the nose stagnation point. The pressure increases rapidly behind the shock wave, but the temperature increases slightly, staying almost unchanged in the induced region,

and then continues to rise rapidly at the position $x/r=-1.12$. The pressure and temperature distributions in this test case match well with those in Ref. [19]. The comparison of the mass fraction distributions of H_2, O_2 and H_2O along the stagnation line is demonstrated in Fig. 6(b), where we can observe clearly that the combustion occurs at the position $x/r=-1.12$ with the decrease of mass fraction of H_2 and O_2 and increase of H_2O. The mass fraction distributions of the species in this test case also match well with the reference data[19].

2.3 Mixed reacting flow around a sphere with an opposing jet of hydrogen

The radius of the sphere and the jet spout is 0.025 m and 0.002 m, respectively, and the computational grid is a 210×129 structured grid (Fig.7). The free stream is composed by the species of N_2 and O_2, and the jet flow is composed by hydrogen. The associated conditions are given in Table 3. The wall is assumed to be adiabatic and non-catalytic. The chemical reactions and the rate coefficients in Arrhenius formula are given in Table 4, and the backward rates of reaction 8 to 14 are calculated by equilibrium constants. In addition, the premixed flow without chemical reactions and the reacting flow considering only the combustion of hydrogen are also simulated under the same conditions.

Fig.8 shows the main features of the flow field

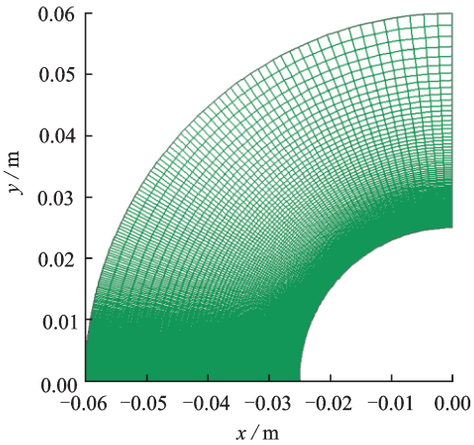

Fig.7 Computational grid

Table 3 Free stream and jet conditions

Ma_∞	p_∞/Pa	T_∞/K	Ma_j	P_{js}/Pa	T_{js}/K
10.0	1 197.03	226.51	1.0	3.0E+5	250

in terms of the Mach number. The flow field is characterized by the detached shock wave, Mach disk and recompression shock wave. And the recirculation region with separation bubble is formed due to the jet interference in the hypersonic free stream. The flow field structure obtained in this paper matches well with that in Ref. [20].

Two characteristic lines for the comparison of the parameter distributions is illustrated in Fig. 9, where the first line passes through the center of the jet with the polar angle of $\theta=0°$, and the second line crosses over the recirculation region with the po-

Table 4 Chemistry model for air chemical reactions and H_2-O_2 combustion

No.	Reaction	Forward rate coefficient/($cm^3/\cdot mol^{-1}\cdot s^{-1}$)	Backward rate coefficient/($cm^3/\cdot mol^{-1}\cdot s^{-1}$)
1	$O_2+M\Leftrightarrow 2O+M$	$3.61\times10^{18}T^{-1.0}\exp(-118\,028/RT)$	$3.01\times10^{15}T^{-0.5}$
2	$N_2+M\Leftrightarrow 2N+M$	$1.92\times10^{17}T^{-0.5}\exp(-224\,730/RT)$	$1.09\times10^{16}T^{-0.5}$
3	$NO+M\Leftrightarrow N+O+M$	$3.97\times10^{20}T^{-1.5}\exp(-150\,217/RT)$	$1.01\times10^{20}T^{-1.5}$
4	$N_2+O\Leftrightarrow NO+N$	$6.75\times10^{13}\exp(-74\,513/RT)$	1.50×10^{13}
5	$NO+O\Leftrightarrow O_2+N$	$3.18\times10^{9}T^{1.0}\exp(-39\,144/RT)$	$9.63\times10^{11}T^{0.5}\exp(-7\,153/RT)$
6	$N_2+N\Leftrightarrow 2N+N$	$4.15\times10^{22}T^{-1.5}\exp(-260\,297/RT)$	$2.32\times10^{21}T^{-1.5}$
7	$N+O\Leftrightarrow NO^++e^-$	$9.03\times10^{9}T^{0.5}\exp(-64\,379/RT)$	$1.80\times10^{19}T^{-1.0}$
8	$H_2+O_2\Leftrightarrow OH+OH$	$1.70\times10^{13}\exp(-48\,150/RT)$	—
9	$H+O_2\Leftrightarrow O+OH$	$1.42\times10^{14}\exp(-16\,400/RT)$	—
10	$OH+H_2\Leftrightarrow H_2O+H$	$3.16\times10^{7}T^{1.8}\exp(-3\,030/RT)$	—
11	$O+H_2\Leftrightarrow OH+H$	$2.07\times10^{14}\exp(-13\,750/RT)$	—
12	$OH+OH\Leftrightarrow H_2O+O$	$5.50\times10^{13}\exp(-7\,000/RT)$	—
13	$H+OH+M\Leftrightarrow H_2O+M$	$2.21\times10^{22}T^{-2}$	—
14	$H+H+M\Leftrightarrow H_2+M$	$6.53\times10^{17}T^{-1}$	—

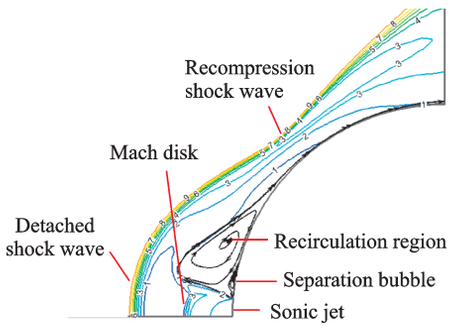

Fig. 8 Mach number distribution and representative streamlines

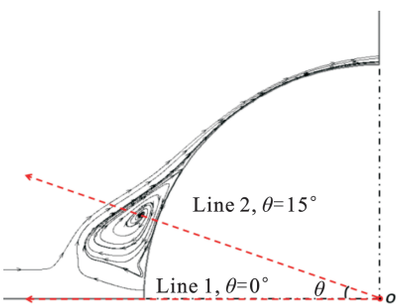

Fig.9 Characteristic lines with the polar angle of θ

lar angle of $\theta = 15°$.

Fig.10(a) shows the temperature distributions along the first characteristic line. The temperature increases rapidly behind the detached shock wave, and then decreases swiftly mixing the cold jet of hydrogen. The maximum value of the temperature in the premixed flow is about 4 095.9 K, while the values of the reacting flow are lower, and the temperature peaks of the reacting flow shift slightly to the negative direction of the x-axis due to the effects of chemical reactions. Figs.10(b), (c) show the mass fraction distributions of the major species (H_2, O_2, H_2O) and minor species (O, H) in the reacting flow, but the peak value of the mass concentration of H_2 is not given in order to display clearly the variation of the mass fraction of the species with low magnitude, which approaching to the jet condition with the value of 1.0. The value of the oxygen mass fraction decreases while the hydrogen mass fraction increases in the mixing layer, and the ratio of oxygen to hydrogen (H_2/O_2) is about 8.59 and 26.36 of the combustion flow and mixed reacting flow, respectively at the peak position of water. Compared with the combustion flow, the maximum values of the mass fraction of water and atomic hydrogen are greater, and the peak mass fraction of the atomic oxygen is one order higher of the mixed reacting flow. The results indicate that the dissociation of oxygen molecule is intense and the production of water is augmented by the effects of air chemical non-equilibrium.

The same parameter distributions along the sec-

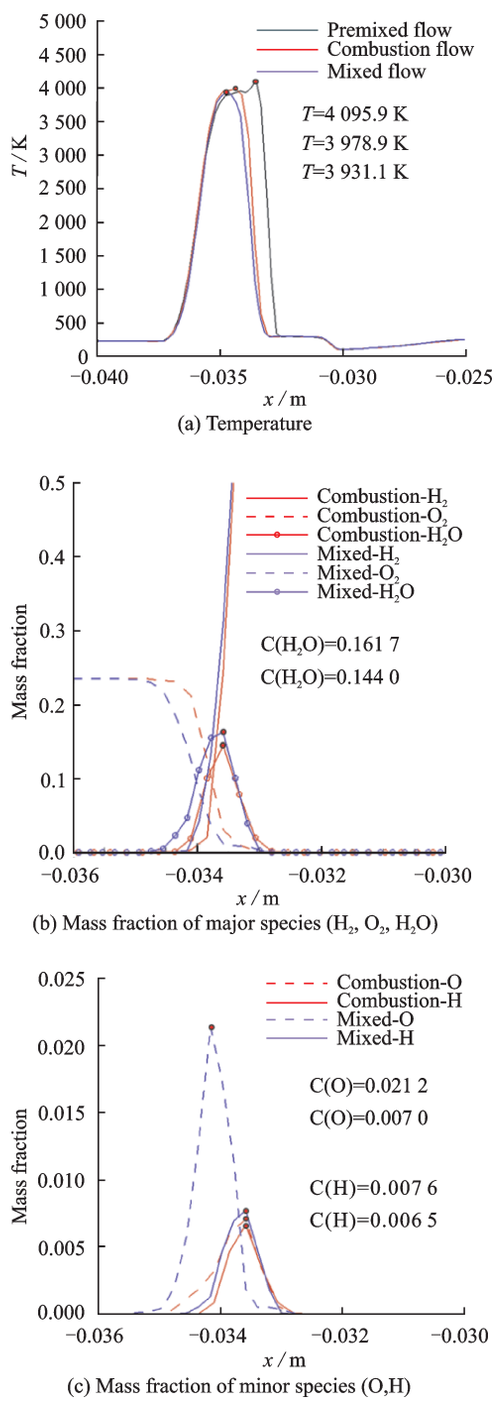

Fig. 10 Comparison of parameter distributions along the line with polar angle of $\theta = 0°$

ond characteristic line are given in Fig. 11, which the peak value of the mass fraction of H_2 is also not given. The maximum value of the temperature in the premixed flow is about 3 740.7 K, which is much lower than that on the first characteristic line, and the effects of chemical reactions also result in the decrease of the peak temperature. The ratio of oxygen to hydrogen is about 0.93 and 2.16 of the combustion flow and mixed reacting flow respectively at the peak position of water. Compared with the combustion flow, the maximum values of the mass fraction of water and atomic hydrogen are less, and the peak mass fraction of the atomic oxygen is greater of the mixed reacting flow. The results indicate that the dissociation of oxygen molecule is weak and the production of water is weakened by the effects of air chemical non-equilibrium.

Fig. 12 shows the comparison of the pressure and temperature distributionson the surface as a function of the polar angle, where the value of $\theta=0°$ means the center of the jet. The value of the peak pressure on the surface of the premixed flow is about 82.7 kPa. The effects of chemical reactions result in the decrease of peak pressure on the surface, and the pressure peaks of the reacting flow shift slightly to the downstream of the jet. The tempera-

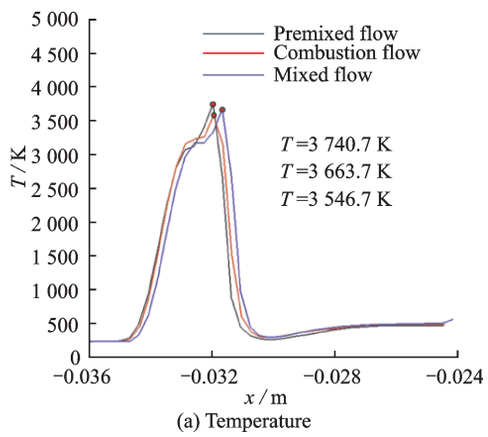

(a) Temperature

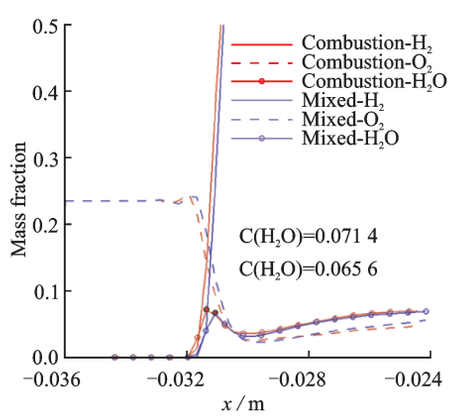

(b) Mass fraction of major species (H_2, O_2, H_2O)

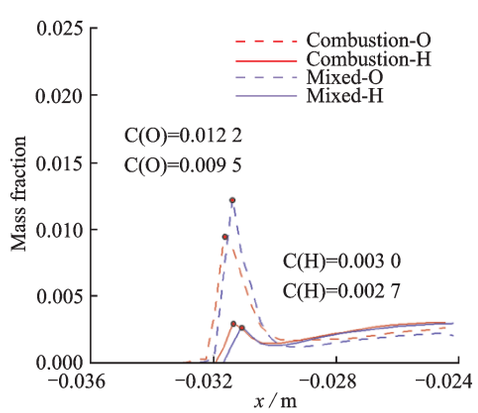

(c) Mass fraction of minor species (O, H)

Fig. 11 Comparison of parameter distributions along the line with polar angle of $\theta=15°$

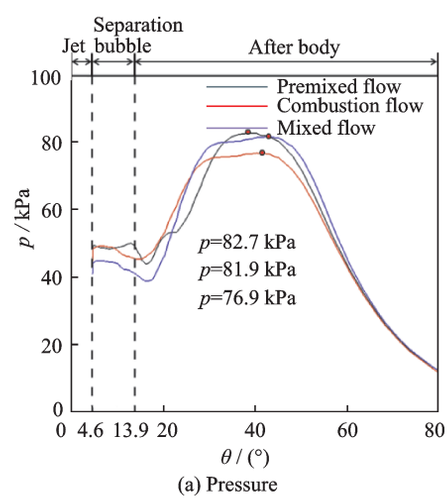

(a) Pressure

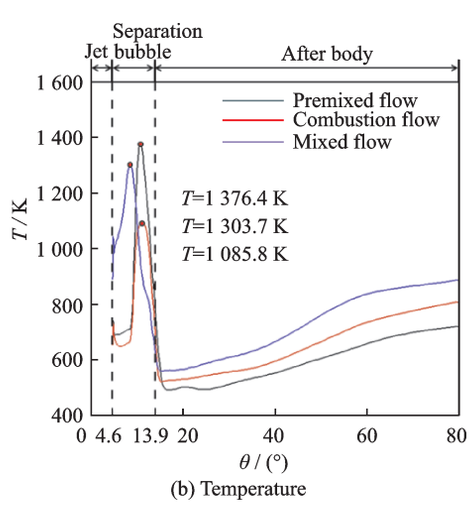

(b) Temperature

Fig.12 Comparison of surface parameter distributions

ture peaks on the surface locate in the region of the separation bubble, and the maximum value of the temperature of the premixed flow is about 1 376.4 K. The peak temperature decreases due to the effects of chemical reactions, especially considering only the combustion of hydrogen.

3 Conclusions

The effects of chemical reactions in the hypersonic reacting flow are investigated using an integrated algorithm considering simultaneously the air chemical reactions and the H_2-air combustion reactions. The program is validated by the hypersonic air non-equilibrium flow of the RAM C-II configuration and the shock-induced combustion flow around a sphere, respectively. After that, the mixed reacting flow with an opposing jet of hydrogen is analyzed. The results show that the program is reliable, and the chemical reactions result in the decrease of peak temperature and peak pressure on the surface under the conditions in this paper. The production of water is augmented in the region with high ratio of oxygen to hydrogen and weakened in the area with low ratio of oxygen to hydrogen by the effects of air chemical non-equilibrium.

The air non-equilibrium flow combined with hydrocarbon-air combustion is under investigation, and will be used to analyze the flow field of hypersonic vehicles with the multi-species reaction control system, as well as the combustion flow field inside the scramjet engine.

References

[1] CANDLER G, MACCORMACK R. The computation of hypersonic ionized flow in chemical and thermal non-equilibrium [C]// 26th AIAA Aerospace Sciences Meeting. Reno: AIAA, 1988.

[2] GAO Zhenxun, JIANG Chongwen, LEE Chunhian. Aeroheating study of hypersonic chemical nonequilibrium flow around a reentry blunt body [C]//AIAA SPACE Conference and Exposition. San Diego: AIAA, 2014.

[3] PARK C. Review of chemical-kinetic problems of future NASA missions, I: Earth entries [J]. Journal of Thermophysics and Heat Transfer, 1993, 7(3): 385-398.

[4] GNOFFO P, GUPTA R, SHINN J. Conservation equations and physical models for hypersonic air flow in thermal and chemical nonequilibrium [R]. NASA-TP-2867, 1989.

[5] BUSSING T, EBERHARDT S. Chemistry associated with hypersonic vehicles [J]. Journal of Thermophysics and Heat Transfer, 1989, 3(3): 245-253.

[6] REDDY D, SINHA K. Effect of chemical reaction rates on aeroheating predictions of reentry flows [J]. Journal of Thermophysics and Heat Transfer, 2011, 25(1): 21-33.

[7] GUPTA R, YOS J, THOMPSON R. A review of reaction rates and thermodynamic and transport properties for an 11-species air model for chemical and thermal non-equilibrium calculations to 30 000 K [R]. NASA-TM-101528, 1989.

[8] OUYANG Shuiwu, XIE Zhongqiang. Navier-Stokes computation of non-equilibrium chemically reacting flow fields [J]. Chinese Journal of Computational Physics, 1997, 14(1): 7-12. (in Chinese)

[9] PARK C. Assessment of two-temperature kinetic model for ionizing air [J]. Journal of Thermophysics and Heat Transfer, 1989, 3(3): 233-244.

[10] RONALD S. A century of ramjet propulsion technology evolution [J]. Journal of Propulsion and Power, 2004, 20(1): 27-58.

[11] WANG Jiangfeng, WU Yizhao, JI Weidong, et al. Progress in numerical simulation techniques of hypersonic aerodynamic problems [J]. Acta Aeronautica et Astronautica Sinica, 2015, 36(1): 159-175. (in Chinese)

[12] CAI Guobiao, XU Dajun. Hypersonic vehicle Technology [M]. Beijing: Chinese Science Press, 2012. (in Chinese)

[13] McClinton C, Rausch V, Nguyen L, et al. Preliminary X-43 flight test results [J]. Acta Astronautica, 2005, 57(2): 266-276

[14] OUYANG Shuiwu, XIE Zhongqiang. High temperature nonequilibrium air flow [M]. Beijing: Chinese National Defense Industry Press, 2001. (in Chinese)

[15] ANDERSON J. Hypersonic and high temperature gas dynamics [M]. New York: McGraw-Hill, 1989.

[16] ZHANG Xianghong, WU Yizhao, WANG Jiangfeng. Numerical simulation of thermo-chemical non-equilibrium hypersonic flow using HLLE+ scheme [J]. Journal of Nanjing University of Aeronautics and Astronautics, 2011, 43(2): 154-158. (in Chinese)

[17] SHANG H, CHEN Y, PAUL L, et al. Investigation of chemical kinetics integration algorithms for reacting

flow [C]//33rd Aerospace Sciences Meeting and Exhibit. Reno: AIAA, 1995.

[18] LEHR H. Experiments on shock-induced combustion [J]. ACTA Astronautica, 1972, 17(4): 589-597.

[19] SOERTRISNO M, IMAY S. Simulation of the flow field of a ram accelerator [C]//27th Joint Propulsion Conference. Sacramento: AIAA, 1991.

[20] HAYASHI K, ASO S, TANI Y. Numerical study of thermal protection system by opposing jet [C]//43rd AIAA Aerospace Sciences Meeting and Exhibit. Reno: AIAA, 2005.

Acknowledgements This work was supported by the Fundamental Research Funds for the Central Universities (No. NZ2016101) and the Priority Academic Program Development of Jiangsu Higher Education Institutions (PAPD).

Authors Mr. **ZHAO Faming** is a Ph.D. candidate in the College of Aerospace Engineering, Nanjing Unlversity of Aeronautls and Astronautics. His research interests focus on the numerical simulation of hypersonic reacting flows.

Prof. **WANG Jiangfeng** received his Ph.D. degree in Computational Fluid Dynamics from Nanjing University of Aeronautics and Astronautics in 2000. His research interests focus on the layout design of hypersonic vehicles, numerical techniques of complex combustion flows, and computational techniques of aerodynamic heating.

Mr. **FAN Xiaofeng** is a Ph.D. candidate in the College of Aerospace Engineering, Nanjing Unlversity of Aeronautls and Astronautics. His research interests focus on the nume-rical simulation of combustion flows of gaseous and liquid fuel.

Mr. **YANG Tianpeng** is a Ph.D. candidate in the College of Aerospace Engineering, Nanjing Unlversity of Aeronautls and Astronautics. His research interests focus on the numerical simulation of hypersonic aerodynamics.

Author contributions Mr. **ZHAO Faming** designed the study, compiled the models, conducted the analysis, interpreted the results and wrote the manuscript. Prof. **WANG Jiangfeng** contributed to the discussion and background of the study. Mr. **FAN Xiaofeng** contributed data and model components for the combustion model. Mr. **YANG Tianpeng** contributed data for the analysis of reactions effects. All authors commented on the manuscript draft and approved the submission.

Competing interests The authors declare no competing interests.

(Production Editor: Zhang Tong)